DOI:
10.1021/acs.langmuir.6b01688

Document Version
Peer reviewed version

Interaction of the anti-microbial peptides Rhesus θ-defensin and porcine protegrin-1 with anionic phospholipid monolayers

Ivana Knyght[1], Luke Clifton[2], Yussif Saaka[1], M Jayne Lawrence[1], David J Barlow*[1]

[1] Institute of Pharmaceutical Science, King's College London, London, SE1 9NH, UK

[2] Rutherford Appleton Laboratory, ISIS Spallation Neutron Source, Harwell OX11 0QX, UK

* Corresponding author:

David J Barlow

E-mail: dave.barlow@kcl.ac.uk

Telephone: 0207 848 4827

Fax: 0207 848 4800

Co-author e-mail addresses

Ivana Knyght: ivana.knyght@kcl.ac.uk

Luke Clifton: l.clifton@stfc.ac.uk

Yussif Saaka: yussif.saaka@kcl.ac.uk

M Jayne Lawrence: jayne.lawrence@kcl.ac.uk

Abstract

A combination of Langmuir isotherm, Brewster angle microscopy (BAM) and neutron reflectivity studies have been performed to gain insight into the effects on model bacterial cell membranes of the antimicrobial peptides, Rhesus θ-defensin 1 (RTD-1) and porcine protegrin 1 (PG-1). The peptides were interacted with monolayers spread at the air-water interface and prepared from a 3:1 molar mixture of phosphatidylethanolamine and phosphatidylglycerol - used to approximate the cell membranes of Gram positive bacteria. The Langmuir film balance measurements show that both peptides perturb the lipid monolayers causing an increase in surface pressure, and the BAM studies show that each results in the formation of small domains within the lipid films, around 5 μm diameter. The overall change in monolayer surface pressure caused by PG-1, however, is a little more pronounced than that due to RTD-1 (+8.5 $mN.m^{-1}$ *vs.* +5.5 $mN.m^{-1}$), and the rate of its initial interaction with the monolayer is a little more rapid than that for RTD-1. The neutron reflectivity studies also show differences for PG-1 and RTD-1, with the model fits to these data showing that the more amphiphilic PG-1 becomes fully embedded within the lipid film – causing an extension of the lipid acyl chains but leaving the thickness of the lipid head group layer unaffected – while RTD-1 is seen to insert less deeply – causing the same extension of the lipid acyl chains as PG-1 but also causing a significant increase in thickness of the lipid head group layer. The various differing effects of the two peptides on anionic lipid monolayers are discussed in the context of their differing haemolytic activities, and their proposed differing propensities to form transmembrane pores.

[275 words]

Keywords

Anti-microbial peptide, protegrin-1, Rhesus theta-defensin-1, Brewster angle microscopy, neutron reflectivity

Introduction

The rapid rise in the frequency of diagnosed microbial infections accompanied by the increased frequency with which these infections prove resistant[1] to the existing arsenal of antibiotics has led to an urgent call for the development of new antimicrobial therapies[2]. The θ-defensins are seen as particularly promising in this respect[2]. These are newly discovered peptides that form part of the innate immune response[3-6] in Old World monkeys and orangutans[6,7]. They are small, arginine rich, relatively inflexible peptides involving 18 residues arranged with N-to-C-terminal main chain cyclization, and stabilised by three disulfide bridges[5] (Figure 1). To date, there are two members of the family that have been characterized structurally, *viz.*, Rhesus θ-defensin-1 (RTD-1)[6] and retrocyclin-2 (HTD-2)[8]. The small size, high stability, and multiple host defence activities of the θ-defensins make them intriguing potential therapeutic agents[5].

Although there are no details yet available on the mode of action of these peptides, their close analogues, the protegrins, (which have a similar pattern of disulfide-links but no main chain cyclization) are suggested to form octameric pores in microbial membranes causing uncontrolled ion leakage, decay of transmembrane potential, loss of cell contents, and ultimately cell death[9]. Interestingly, however, the protegrins are shown to cause significant lysis of mammalian red blood cells, whereas the θ-defensins do not[10].

In the experiments reported here, we sought to use a combination of Langmuir isotherm, Brewster angle microscopy and neutron reflectivity studies to gain insight into the mode of action of the θ-defensins and the protegrins, with the specific aim to compare the manner in which these peptides interact with anionic lipid monolayers - which we use to approximate Gram positive bacterial cell membranes.

The studies were conducted using synthetic porcine protegrin-1 (PG-1) and the acyclic (N- and C-terminally capped, but fully disulfide-linked) form of Rhesus θ–defensin-1 (aRTD-1) (see Figure 1), with the concentrations of each peptide (0.48 μM) chosen according to their reported inhibitory potencies (*viz.*, 0.1 – 1 μM)[10,11]. The lipid monolayers used were prepared from a 3:1 molar mixture of phosphatidylethanolamine and phosphatidylglycerol which approximates the cell membranes of Gram positive bacteria[12-13].

Experimental

Materials

2-oleoyl-1-palmitoyl-*sn*-glycero-3-phospho-(1'-*rac*-glycerol) (*h*-POPG, $C_{40}H_{76}O_{10}P$, Mw 770.99 g mol^{-1}), 2-oleoyl-1-d_{31}-palmitoyl-*sn*-glycero-3-phospho-(1'-*rac*-glycerol) (palmitoyl chain deuterated POPG, d_{31}-POPG, $C_{40}H_{45}$ $D_{31}O_{10}P$, MW 802.1 g mol^{-1}), 2-oleoyl-1-palmitoyl-*sn*-glycero-3-phosphoethanolamine (*h*-POPE $C_{39}H_{76}NO_8P$ Mw 718.01 g mol^{-1}) and 2-oleoyl-1-d_{31}-palmitoyl-*sn*-glycero-3-phosphoethanolamine (palmitoyl chain deuterated POPE, d_{31}-POPE, $C_{39}H_{45}$ $D_{31}NO_8P$ MW 749.2 g mol^{-1}) were purchased from Avanti Polar Lipids (Alabaster, AL) and (after checking their purity by comparison of the measured Langmuir isotherms against those reported in the literature) were used as supplied.

Protegrin 1 (PG-1; MW 2157.63 g mol^{-1}) and acyclic Rhesus θ-defensin 1 (aRTD-1; Mw 2100.62 g mol^{-1}) were custom-synthesized to 99 % purity (as characterized by reverse phase HPLC and mass spectrometry; EZ Biolabs, Indiana, USA) and were used as received. aRTD-1 has the same sequence and disulfide topology as the natural RTD-1 peptide but lacks main chain cyclisation and has its N- and C-termini capped by acetyl and amide groups, respectively.

Ethanol, chloroform (spectroscopic grade) and D_2O (99.9% deuteration) were purchased from Sigma Aldrich (Poole, Dorset, UK). Ultrapure water (with resistivity, 18.2 MΩ.cm at 25°C) was obtained from a Millipore Milli-Q system (Millipore, Billerica, MA, USA).

Surface-pressure area (π - *A*) isotherms

Langmuir surface pressure measurements were recorded using a Nima Technologies 601 Langmuir trough (Nima Technologies, Coventry, UK). After cleaning with copious amounts of water, followed by ethanol and then chloroform, the trough was filled with 130 mL ultrapure water. Lipid monolayers (POPE:POPG in 3:1 molar ratio) were spread onto the surface of the subphase from chloroform solution (at a concentration of 1 mg mL^{-1}) using a Hamilton syringe (Bonaduz, Switzerland). The chloroform was allowed to evaporate for 10 minutes after which time the resultant lipid monolayer was compressed (at 30 cm^2 min^{-1}) to determine the isotherm while continually recording surface pressure by means of a

Wilhelmy plate (10 mm x 50 mm Whatman No. 1 filter paper; Whatman International, Maidstone, UK) partially submersed in the aqueous subphase.

In order to establish the extent and kinetics of interaction of the anti-microbial peptides with the POPE:POPG monolayer, a lipid film was spread and compressed to a surface pressure of 25 mN m^{-1}. The stability of the monolayer was subsequently confirmed by holding at constant area and monitoring for changes in surface pressure over a period of 30 minutes. With the monolayer seen to be stable, an aqueous solution of PG-1 or aRTD-1 was systematically injected, slowly and evenly, into the aqueous sub-phase, such that the final concentration of peptide in the trough was 0.48 μM. The surface pressure of the lipid film after injection of the peptide was then continuously monitored to ensure that any change in surface pressure due to the presence of the peptide had completed. In all cases, the time course of the interaction was found to be complete within ~90 minutes.

All Langmuir film balance experiments were performed in triplicate using a freshly prepared monolayer each time.

Brewster angle microscopy

Brewster angle micrographs were obtained using a BAM2plus microscope (Nanofilm Technology, Goettingen, Germany) mounted above a Langmuir trough (Model 302m, Nima Technology Ltd, Coventry, UK) equipped with a surface pressure sensor. The microscope was equipped with a frequency doubled Nd:YaG laser (532 nm, 20 mW), polarizer, analyser and CCD camera. Lipid monolayers were deposited as described for the neutron reflectivity studies. Once equilibrated at 25 $mN.m^{-1}$, an aqueous solution of anti-microbial peptide (either PG-1 or aRTD-1) was added to the subphase to give a subphase concentration of 0.48 μM. The surface pressure and film structure were then monitored for 3 hours following peptide addition. BAM images, taken at regular intervals following the peptide addition, were obtained using a 10x objective, providing a final magnification of x15, with image dimensions 392 μm by 503 μm.

Neutron reflectivity studies

Measurements of the monolayer neutron reflectivity, $R(Q)$, were obtained as a function of the scattering vector, Q, ($Å^{-1}$, $Q = 4\pi\sin\theta/\lambda$, where λ is the neutron wavelength), and the data collected on the INTER reflectometer in TS2 at the STFC Rutherford Appleton Laboratory (Chilton, Oxfordshire, UK). Measurements were made with incident angles, θ = 0.8° and 2.3°, giving a Q-range of 0.014 – 1 $Å^{-1}$. (It should be noted here, however, that although the reflectivity measured at $Q < 0.03$ $Å^{-1}$ serves little benefit in modeling the structures of the various interfacial lipid and lipid/peptide layers, it does give confidence that the reflectivities are scaled correctly – as evidenced by the critical edge observed for D_2O.)

Instrument calibration was performed using a pure D_2O subphase. For all systems studied, the neutron reflectivity measurements were recorded at 298 ± 2 K, and the data obtained under the three isotopic contrasts of: *h*-POPE:POPG monolayer on D_2O, *d*-POPE/POPG monolayer on D_2O, and *d*-POPE/POPG monolayer on null reflecting water (nrw; 92% v/v H_2O:D_2O).

The neutron reflectivity experiments were performed under the same experimental conditions and using the sample environments as employed in the measurement of the surface pressure-area (π - A) isotherms. The POPE:POPG monolayer films were compressed at a rate of 30 cm^2 min^{-1} to a surface pressure of 25 mN m^{-1} and the film then maintained at constant area for the duration of the reflectivity experiment.

After measuring the reflectivity of each lipid film (and ensuring that it was fully consistent between the repeat experiments), the compressed monolayer was maintained at the same area while constantly monitoring surface pressure, exposed to aRTD-1 or PG-1, and the reflectivity re-measured in 10 min time slices until it was clear that there were no further changes in reflectivity. The time for re-equilibration of the films after exposure to the antimicrobial peptides – as judged from the monitoring of the neutron reflectivity – was found consistent with that judged from the change in surface pressure, and was typically about 2 hours. After re-equilibration, the reflectivity profiles for the lipid films were recorded as previously.

Neutron reflectivity data analysis

Reflectivity data were reduced using Mantid[14], and the reduced data analysed using the Abeles optical matrix methodology, with exploratory fits initially performed for the individual data sets using Afit (http://rkt.chem.ox.ac.uk/afit.html), and simultaneous refinements against all three contrasts subsequently carried out using Motofit (http://sourceforge.net/projects/motofit/). The scattering length densities and molecular volumes of materials are summarized in Table 1. For the peptides aRTD-1 and PG-1, the scattering length densities in nrw and D_2O were computed on the basis of 46 and 51 polar/exchangeable protons, respectively. Fits were performed assuming a Q-resolution of 1%, and background scattering appropriate (and consistent) for the aqueous sub-phase under consideration (*viz.,* ~4 x 10^{-6} Å^{-2} for D_2O and ~6 x 10^{-6} Å^{-2} for nrw.

The fitted scattering length density for each neutron contrast was related to the volume fractions of its various components as:

Equation 1:

$$\rho_L = \left(\rho_{lipid} \cdot \varphi_{lipid}\right) + \left(\rho_{pep} \cdot \varphi_{pep}\right) + \left(\rho_{solvent} \cdot \varphi_{solvent}\right)$$

where ρ_L is the fitted scattering length density of a given layer (Å^{-2}), $\rho_{solvent}$, ρ_{pep}, and ρ_{lipid} are respectively the scattering length density of the solvent, peptide, and 3:1 POPE:POPG mixture (Å^{-2}), and ϕ are the corresponding component volume fractions.

The interfacial molecular area for a given component (A, Å^2) within a given layer was calculated as:

Equation 2:

$$A = \frac{\Sigma b}{\left(\tau \cdot \varphi \cdot \rho\right)}$$

where ϕ and ρ are respectively the volume fraction of the component within the layer and its scattering length density, Σb is the sum of the component's atomic scattering lengths (Å), and τ is the fitted layer thickness (Å). The surface excess of peptide within a given layer (Γ, mg.m^{-2}) was obtained as:

Equation 3:

$$\Gamma = \frac{MW}{A \cdot 6.02}$$

where *MW* is the relative molecular mass of the peptide and *A* its interfacial molecular area within the layer.

The molecular volumes of aRTD-1 and PG-1 were computed from their relative molecular masses assuming a standard protein density[15] of 1.37 g.cm^{-3}.

Results and Discussion

Surface-pressure area (π - *A*) isotherms

The isotherms recorded for the *h*- and d_{31}-POPE/POPG monolayers (Figure 2a) exhibit no marked phase transition and are consistent with those reported by previous workers[16]. At a surface pressure of 25 mN.m^{-1} – as used in the subsequent neutron reflectivity experiments – both the *h*- and d_{31}-POPE/POPG monolayers exist in an expanded phase with a mean interfacial molecular area (calculated from the isotherm) of a_0 ~70 Å^2. There are differences seen in the isotherms recorded for the *h*-lipid and d_{31}-lipid films only when the films are highly compressed – when the mean interfacial area falls below 60 Å^2 – and this is as might be expected given the subtle differences in inter-atomic interactions for protiated *vs*. deuterated alkyl chains[17].

With a 3:1 POPE/POPG monolayer compressed to a surface pressure of 25 mN.m^{-1} and then held at constant area, kinetic experiments following the addition of 0.48 μM aRTD-1 into the sub-phase indicate an interaction of the peptide with the lipid film, with the addition causing an increase in surface pressure of around 5.5 mN.m^{-1}, and film equilibrium re-established roughly 2 hours post-injection (Figure 2b). The equivalent experiments performed for PG-1 (Figure 2c) also testify to an interaction of the peptide with the lipid film, with the surface pressure in this case changing by a total of about 8.5 mN.m^{-1}, and the changes in the film again complete after roughly 2 hours.

Comparable experiments reported for other anti-microbial peptides – albeit using monolayers with differing lipid compositions – give broadly similar results. The interactions

of β-purothionin and puroindoline-a with DPPG monolayers compressed to 22 $mN.m^{-1}$, are shown (under the same conditions and using the same experimental set-up) to cause increases in surface pressure of 14 $mN.m^{-1}$ and 10 $mN.m^{-1}$, respectively, with the film re-equilibrating in each case after about 3 hours[18]. Increases in surface pressure in the range 9 – 20 $mN.m^{-1}$ are reported for the interaction of melittin, magainin II and cecropin P1 with DPPG monolayers (compressed to 20 $mN.m^{-1}$), with film equilibrium following interaction of all three of these peptides re-established after 1 – 3 hours[19]. The interaction of bactenecin[20] with a mixed DPPC/DPPG monolayer compressed to 25 $mN.m^{-1}$ and that of dicynthaurin[21] with a DPPG monolayer compressed to 25 $mN.m^{-1}$ result in surface pressure changes of +8 $mN.m^{-1}$ and +10 $mN.m^{-1}$, respectively, with both of these changes complete within 1 – 2 hours. It would thus appear that the overall changes in surface pressure induced by the various anti-microbial peptides are much the same, regardless of the exact composition and compression state of the anionic lipid monolayers, and also seemingly independent of the differing size and amphipathicity of the interacting peptides.

From the surface pressure-time plots obtained following exposure of the monolayers to PG-1 and aRTD-1, we do see, however, that there are differences in the kinetics of the *initial* interactions of these two peptides with the lipid monolayers, with the latter causing a change in surface pressure of ~3 $mN.m^{-1}$ within the first half-hour following exposure, and aRTD-1 causing a change of only half this in the same time period. This difference in the initial rates of the two peptides' interactions might perhaps be explained by the fact that PG-1 is significantly more amphiphilic than aRTD-1, and will thus more readily insert itself in the monolayer at the hydrophobe-head group (air-water) interface, whereas aRTD-1's interaction with the monolayer will be dictated mainly by the electrostatic interaction between its multiple cationic side chains and the anionic groups in the monolayer, so that it associates – initially, at least – only with the phospholipid head groups.

The timescales of the events that conspire to account for the rather slow kinetics of the peptides' interaction with the lipid monolayers and the long times taken subsequently for the monolayers to re-equilibrate, include the time taken for the peptides to diffuse to the interface from the bulk, the time required on their arrival at the interface to insert into the monolayer, and the time then required for them to re-arrange (both laterally and vertically) once inserted into the monolayer.

Brewster Angle Microscopy

In the absence of the antimicrobial peptides, the BAM images of the 3:1 POPE:POPG monolayers appear to show some form of liquid phase separation, with the film presenting as a raft of irregularly packed, roughly circular domains ranging in size from 10 – 50 μm diameter (see Figure S1A, Supplementary Information).

After exposure to aRTD-1 and PG-1 (the BAM images in these two cases appearing much the same), there are bright ~5 μm domains that appear in the lipid film (see Figure S1B, Supplementary Information). It is impossible to determine the nature/composition of these domains from a simple inspection of the BAM images, but we speculate that they might perhaps be due to peptide aggregates formed within the monolayer, or they might arise as the result of a peptide-induced formation of condensed phase areas within the lipid film. The antimicrobial peptides clearly, therefore, introduce heterogeneity in the lipid films but it is important to note here that – from the point of view of the neutron reflectivity measurements – the sizes of these domains are significantly smaller than the neutron coherence length (*viz*., ~5 μm *vs*. 20–40 μm), and we can be confident, therefore, that any diffuse scattering that arises from the domains will make an insignificant contribution to the measured neutron specular reflection; the model fits to these data can thus be safely assumed to represent an average for the monolayer.

Neutron reflectivity

3:1 POPE:POPG monolayer structure

Modelling of the reflectivity data for the 3:1 POPE:POPG monolayers was performed assuming a two-layer structure, with layer 1 (on the air-side) containing the lipid palmitoyl and oleoyl chains, and layer 2 (on the sub-phase side) containing the phosphatidylethanolamine (PE) and phosphatidylglycerol (PG) head groups. Fitting was performed with the scattering length densities for the two layers fixed as appropriate to these assumed lipid contents, and with optimization of the thickness and percent solvent in each of the layers, with the roughness at each interface set to zero. The final set of fitted parameter values are presented in Table 2.

A mean interfacial molecular area of 70 ± 2 Å^2 is calculated on the basis of the fitted layer thicknesses and scattering lengths, and this tallies with our own isotherm estimate of the area (*vide supra*), but is a little higher than the areas reported (on the basis of Langmuir film balance measurements) for 3:1 POPE:POPG monolayers by Picas *et al.*[16] (68 Å^2) and Suárez-Germà *et al*.[22] (66 Å^2).

The thickness of the lipid acyl chains layer (layer 1) was fitted as 13 ± 1 Å, and this compares favourably with the values quoted in the literature for POPC and POPG (in both cases, ~13.5 Å)[23,24]. Assuming extended chain lengths of 16.4 Å and 15.9 Å for the C16:0 and C18:1 chains, respectively, such a layer thickness indicates that the chains are tilted by around 35^o – 37^o with respect to the normal to the air-water interface. For comparison, we note that the chain tilts recorded by Huynh *et al*[25] in their molecular dynamics simulations of POPC monolayers are in the range 35^o – 43^o.

Our fitted PE/PG head group layer (layer 2) thickness is obtained as 9 ± 1 Å, and this is consistent with the layer thickness suggested by Kucerka *et al*[23]. The reflectivity-derived head group hydration is calculated as 7 H_2O per lipid, and again this compares favourably with the experimentally determined figure of 9.4 H_2O quoted for POPC by Kucerka *et al*[23], and the figure of 6 – 7 H_2O per lipid derived from molecular dynamics simulations of a 3:1 POPE:POPG monolayer reported by Murzyn *et al*[26].

<u>3:1 POPE:POPG monolayer structure after exposure to aRTD-1 and PG-1</u>

Simultaneous fittings of the reflectivity profiles obtained after exposure of the 3:1 POPE/POPG monolayer to aRTD-1 and PG-1 were first performed using a three-layer model in which the values of the parameters for the first two layers were fixed as found for the monolayer before exposure to the peptides, and the scattering length density of the third layer fixed as calculated for the added peptide, and with simultaneous fitting of the reflectivity profiles performed with optimisation only of the thickness and solvent content of layer 3. These model fits, however, were found to be statistically very poor and/or physically unreasonable (data not shown).

Two-layer (rather than three-layer) simultaneous fits were thus carried out in which the values of the parameters for layer 1 were fixed as obtained for the acyl chains layer (layer 1) in the monolayer prior to exposure to the peptides, and the parameters (of thickness,

scattering length density, and solvent content) for the second (solvent-side) layer optimised in the fitting process. The resulting fitted parameter values for the monolayers exposed to aRTD-1 and PG-1 are both summarized in Table 2, and the fits to the reflectivity profiles for the monolayers before and after their exposure to aRTD-1 are shown in Figure 3.

With these models, it was found that exposure of the monolayer to either of the two anti-microbial peptides resulted in an increase in the thickness and water content of the lipid head group layer, with the magnitude of these changes different for PG-1 and aRTD-1, but with both peptides "associated with" ~6 lipid molecules. The greater increase in the thickness of layer 2 caused by aRTD-1 compared with that caused by PG-1 (+8.5 Å *vs*. +5.5 Å; Table 2) could perhaps be attributed to the greater rigidity of aRTD-1. It is less easy, however, to account for the differing effects of the two peptides on the level of monolayer hydration: PG-1 is seen to cause a smaller increase in the monolayer solvent content compared with that due to aRTD-1 (+6% *vs*. +17%; Table 2) and yet it has eight charged groups and a net charge at pH 7 of +6, while aRTD-1 has only 5 charged groups and a net charge of only +5 at pH 7. Moreover, on the basis of grazing incidence X-ray diffraction and specular X-ray reflectivity studies of compressed DPPG films, Neville *et al* have previously reported that PG-1 inserts into both the lipid head group *and* the acyl chains layers of a DPPG monolayer[27]. This observation was consistent with those reported by Ishitsuka *et al* – where (on the basis of Langmuir trough and fluorescence microscopy studies) PG-1 was shown to disturb the tail group packing and by inference to insert into the monolayers formed by DPPE and DPPG (at 25 mN/m)[28]. Similar models of peptide interaction with DPPG monolayers have also been reported by Clifton *et al*[29] and Sanders *et al*[30] in their neutron reflectivity studies of the membrane interactions of purothionin and puroindoline, and by Lad *et al*[19] in their combined FTIR and neutron reflectivity study of melittin interaction with DPPG monolayers. (Attempts to improve these two-layer models by physically meaningful increases in the roughness of one or both of the layers proved unsuccessful.)

Given the various findings reported by previous researchers, therefore, and despite the satisfactory quality of the data fits obtained with our two-layer modeling of the structures of the POPE/POPG monolayers after exposure to aRTD-1 and PG-1, we proceeded to perform further fitting of the reflectivity profiles – seeking consistency with the earlier results – assuming the presence of peptide in both the acyl chains layer and the head

groups layers in the monolayer. In these fits, the thickness, scattering length density, and solvent content of each of the two layers were optimized.

These new fitted models were found to be different for the monolayer exposed to aRTD-1 compared with that exposed to PG-1 and the fitted parameter values are summarized in Tables 3 and 4. Figure 4 shows the fitted neutron reflectivity data for the monolayer exposed to PG-1, and the volume fractions of the components of the layers after exposure to aRTD-1 and PG-1 are summarized in Table 5.

Note here that the quality of these alternative two-layer fits is little different from that achieved with those performed assuming peptide only in the lipid head group region of the monolayer but they are preferred over our earlier models, in part because they are consistent with the findings reported by previous researchers[27,28], and also because they account for the known differences in structures and biological properties of PG-1 and aRTD-1 (see below).

After exposure of the POPE/POPG monolayer to aRTD-1, there is a change in thickness seen for both the acyl chains layer (layer 1) and the head groups layer (layer 2), the former increasing by 3.6 Å, and the latter by 8.8 Å. There are changes too in the scattering length densities of the two layers, and these are consistent with peptide volume fractions of 0.15 in layer 1 and 0.113 in layer 2. The volume fractions of lipid acyl chains in layer 1 is 0.85 and the volume fraction of lipid head groups in layer 2 is 0.187. The average interfacial molecular area of the lipid in the monolayer decreases from 70 $Å^2$ (prior to exposure to the peptide) down to 64 $Å^2$, and the percentage of solvent in the head group layer increases from 33% to 70%. The interfacial molecular areas and surface excesses of the peptide in layers 1 and 2 are 1004 $Å^2$ and 0.34 $mg.m^{-2}$, and 1221 $Å^2$ and 0.29 $mg.m^{-2}$, respectively.

After exposure of the POPE/POPG monolayer to PG-1, the lipid acyl chains layer (layer 1) again increases in thickness from 13 Å to 16.5 Å, but the thickness of the head groups layer (layer 2) remains at 9 Å. The change in scattering length density observed for layer 1 following exposure to PG-1, indicates volumes fractions of peptide and lipid in this layer of 0.15 and 0.85, respectively, the areas per molecule for the lipid and peptide then obtained as 64 $Å^2$ and 1038 $Å^2$ – the latter indicating a PG-1 surface excess in layer 1 of 0.34 $mg.m^{-2}$. In the head groups layer of the monolayer after exposure to PG-1, the volumes fractions of the lipid and peptide are obtained as 0.19 and 0.32, respectively, and these indicate areas

per molecule of 64 Å^2 for the lipid, and 865 Å^2 for the PG-1, with a surface excess of PG-1 in this layer of 0.41 mg.m^{-2}. As was found for the modelling of the reflectivity data assuming PG-1 penetration only into the lipid head group layer, this alternative modelling again shows an increase in the level of head group hydration that is significantly less than seen following exposure to aRTD-1 (increasing only to 49% rather than 70%).

Regardless of whether the POPE/POPG monolayer is exposed to PG-1 or aRTD-1, therefore, we see that the acyl chains layer increases in thickness by around 3.5 Å, indicating that both peptides interact with the lipid film and cause the hydrocarbon chains to assume their fully extended length (~16 Å). The changes that are induced in the lipid head groups layer, however, are clearly very different for aRTD-1 and PG-1. While the former causes the head group layer to more-or-less double in thickness (increasing from 9 Å to 18 Å), the latter appears not to cause any increase in the head group layer thickness. For PG-1, therefore, it would seem that the peptide inserts fully into the monolayer and yet causes only a change in the lateral packing of the lipid molecules (with the result that the mean lipid interfacial area decreases from 70 Å^2 to 64 Å^2). In the case of aRTD-1, however, it would seem that the peptide inserts only partially into the lipid layer, causing the same reduction in the lipid interfacial area, but with a significant part of its structure protruding from the layer and lying within an extended head group layer. The scattering length density profiles calculated for the two peptide-exposed monolayers are shown in Figure 5A, and schematics of their molecular architectures are given in Figures 5B and 5C.

The various differences that are observed here for the effects of PG-1 and aRTD-1 on anionic lipid monolayers are consistent with the reported differences in their hemolytic activities, and also with their proposed differing propensities for transmembrane pore formation. While both θ-defensin and its acyclic variant, aRTD-1, are shown to be essentially non-hemolytic when tested at a concentration of 50 μg.mL^{-1} (that is, a concentration of ~100 μM), PG-1, when tested at the same concentration, is reported to cause a complete loss of erythrocyte viability[31]. The more amphiphilic peptide, PG-1 – with its central β-sheet having distinct hydrophilic and hydrophobic faces – inserts into the lipid monolayer positioning itself at the air-water interface such that its apolar leucine, tyrosine, phenylalanine and valine side chains lie within the lipid acyl chain region, and its cationic arginine side chains interacting with the anionic phosphates of the lipid head groups. In contrast, the relatively

non-amphiphilic aRTD-1, which lacks any clear hydrophobic region, is unable to sit quite as favorably as PG-1 at the air-water interface, and so positions itself primarily within the lipid head group region, thereby causing the head groups to extend and orient themselves to lie more perpendicular to the interface.

The observations recorded here are also consistent with the results obtained in molecular dynamics (MD) simulations[32] of the antimicrobial peptides' interactions with anionic membranes. These MD studies show that the membrane-embedded octameric β-barrels of PG-1 are stable and persistent, causing a localized thinning of the membrane, and forming transmembrane pores of 2 nm inner and 4 nm outer radius. In contrast, the same oligomeric assemblies of RTD-1 are seen to be much less stable, becoming distorted over the course of the simulation and showing peptide molecules migrating out and away from the pore.

Summary and Conclusions

On the basis of the reported Langmuir film balance and neutron reflectivity studies, it is thus concluded that - despite their common classification as cationic β-hairpin antimicrobial peptides - PG-1 and RTD-1 show significant differences in their interaction with anionic lipid monolayers. The more amphiphilic PG-1 appears to become deeply embedded within the anionic lipid monolayer while RTD-1 interacts in a relatively superficial manner, remaining much more intimately associated with the anionic lipid head groups. By extrapolation, it would thus seem reasonable to expect that while RTD-1 would show relatively little interaction with neutral/zwitterionic lipid membranes (as found in eukaryotic cell membranes), PG-1 would interact with this type of membrane much more strongly. We can thus account for the differences between the two peptides that are seen experimentally, with PG-1 recorded as haemolytic, and RTD-1, non-haemolytic[31].

References

1. de Kraker M.E.; Davey, P.G.; Grundmann, H. Mortality and hospital stay associated with resistant *Staphylococcus aureus* and *Escherichia coli* bacteremia: Estimating the burden of antibiotic resistance in Europe**.** *PLoS Med.* **2011,** *2011*, article e1001104.

2. Davies, S.C. (2013) Annual Report of the Chief Medical Officer: Infections and the rise of antimicrobial resistance. London: Department of Health.

3. Zasloff, M. Antimicrobial peptides of multicellular organisms. *Nature* **2002**, *415*, 389 - 395.

4. Yang D.; Biragyn, A.; Hoover, D.M.; Lubkowski, J; Oppenheim, J.J. Multiple roles of antimicrobial defensins, cathelicidins and eosinophil-derived neurotoxin in host defense. *Ann. Rev. Immunol*. **2004**, *22*, 181 - 215.

5. Lehrer R.I.; Cole, A.M.; Selsted, M.E. θ-defensins: cyclic peptides with endless potential. *J. Biol. Chem*. 2012, *287*, 27014 - 27019.

6. Trabi M.; Schirra, H.J.; Craik, D.J. Three-dimensional structure of RTD-1, a cyclic antimicrobial defensin from Rhesus macaque leukocytes. *Biochem*. **2001**, *40*, 4211 - 4221.

7. Nguyen T.X.; Cole, A.M.; Lehrer, R.I. Evolution of primate θ-defensins: a serpentine path to a sweet tooth. *Peptides* **2003**, *24*, 1647-54.

8. Conibear, A.C.; Rosengren, K.J.; Harvey, P.J.; Craik, D.J. Structural characterization of the cyclic cystine ladder motif of θ-defensins. *Biochem*. **2012**, *51*, 9718-9726.

9. Mani, R., Cady, S.D., Tang, M., Waring, A.J. Lehrer, R., Hong, M. (2006) Membrane-dependent oligomeric structure and pore formation of a β-hairpin antimicrobial peptide **in** lipid bilayers from solid-state NMR. Proc. Natl. Acad. Sci. (USA) 103:16242-16247.

10. Tran, D.; Tran, P.; Roberts, K. Osapay, G.; Schaal, J.; Ouellette, A.; Selsted, M.E. Microbicidal properties and cytocidal selectivity of Rhesus macaque theta defensins. *Antimicr. Agents Chemother.* **2008**, *52*, 944 – 953.

11. Steinberg, D.A.; Hurst, M.A.; Fujii, C.A.; Kung, A.D.C.; Ho, F.-C.; Cheng, F.C.; Loury, D.J.; Fiddes, J.C. Protegrin-1: a broad-spectrum, rapidly microbicidal peptide with in vivo activity. *Antimicrob. Agents Chemotherapy.* **1997**, *41*, 1738 – 1742.

12. Lohner, K. Development of novel antimicrobial agents: emerging strategies. K. Lohner (Ed.), The Role of membrane lipid composition in cell targeting of antimicrobial peptides, Horizon Scientific Press, Wymondham, Norfolk, U.K (2001), pp. 149–156.

13. Prossnigg, F.; Hickel, A.; Pabst, G.; Lohner, K. Packing behaviour of two predominant anionic phospholipids of bacterial cytopasmic membranes. *Biophys. J.* **2010**, *150*, 129 – 135.

14. Arnold, et al., Mantid—Data analysis and visualization package for neutron scattering and μSR experiments, Nuclear Instruments and Methods in Physics Research Section A, Volume 764, 11 November 2014, Pages 156-166.

15. Quillin, M.L., Matthews, B.W. Accurate calculation of the density of proteins. *Acta Crystallogr., Sect. D: Biol. Crystallogr.*, **2000**, 56, 791–794.

16. Picas, L.; Suarrez-Germa, C.; Montero, T.; Domenech, O.; Hernandez-Borrell, J. Miscibility behavior and nanostructure of monolayers of the main phospholipids of *Escherichia coli* inner membrane. *Langmuir* **2012**, *28*, 701-706.

17. Calado, J.C.G.; Jancsó, G.; Lopes, J.N.C.; Markó, L.; Nunes da Ponte, M.; Rebelo, L.P.N.; Staveley, L.A.K. The excess thermodynamic properties of liquid CH_4 and CD_4. *J. Chem. Phys.* **1994**, *100*, 4582-4590.

18. Clifton, L.A.; Sanders, M.R.; Hughes, A.V.; Neylon, C.; Frazier, R.A.; Green, R.J. Lipid binding interactions of antimicrobial plant seed defence proteins: puroindoline-a and β-purothionin. Phys. *Chem. Chem. Phys*. **2011**, *13*, 17153-17162.

19. Lad, M.D.; Birembaut, F.; Clifton, L.A.; Frazier, R.A.; Webster, J.R.P.; Green, R.J. Antimicrobial peptide-lipid binding interactions and binding selectivity. *Biophys. J.* **2007**, *92*, 3575-3586.

20. Lopez-Oyama, A.B.; Taboada, P.; Burboa, M.G.; Rodriguez, E.; Mosquera, V.; Valdez, M.A. Interaction of the cationic peptide bactenecin with mixed phospholipid monolayers at the air-water interface. *J. Colloid Interf. Sci.* **2011**, *359*, 279-288.

21. Bringezu, F.; Majerowicz, M.; Maltseva, E.; Wen, S.; Brezesinski, G.; Waring, A.J. Penetration of the antimicrobial peptide dicynthaurin into phospholipid monolayers at the air-water interface. *Chembiochem.* **2007**, *8*, 1038-1047**.**

22. Suárez-Germà, C., Montero, M.T., Ignés-Mullol, J., Hernández-Borrell, J., Oscar, D. Acyl chain differences in phosphatidylethanolamine determine domain formation and LacY Distribution in biomimetic model membranes. *J. Phys. Chem. B* **2011**, *115*, 12778-12784.

23. Kucerka, N.; Tristram-Nagle, S.; Nagle, J.F. Structure of fully hydrated fluid phase lipid bilayers with monounsaturated chains. *J. Membrane Biol.* **2005**, *208*, 193-202.

24. Pan, J.; Heberle, F.A.; Trsitram-Nagle, S.; Szymanski, M.; Koepfinger, M.; Katsaras, J.; Kucerka, N. Molecular structures of fluid phase phosphatidylglycerol bilayers as determined by small angle neutron and X-ray scattering. *Biochim. Biophys. Acta* **2012**, *1818*, 2135-2148.

25. Huynh, L.; Perrot, N.; Beswick, V.; Rosilio, V.; Curmi, P.A.; Sanson, A.; Jamin, N. Structural properties of POPC monolayers under lateral compression: computer simulations analysis. *Langmuir* **2014**, *30*, 564-573.

26. Murzyn, K.; Rog, T.; Pasenkiewicz-Gierula, M. Phosphatidylethanolamine-phosphatidylglycerol bilayer model as a model of the inner bacterial membrane. *Biophys. J.* **2005**, *88*, 1091-1103.

27. Neville, F.; Ishitsuka, Y.; Hodges, C.S.; Konovalov, O.; Waring, A.J.; Lehrer, R.; Yee, K.Y.C. Protegrin interaction with lipid monolayers: grazing incidence X-ray diffraction and X-ray reflectivity study. *Soft Matter* **2008**, *4*, 1665-1674.

28. Ishitsuka, Y.; Pham, D.S.; Waring, A.J.; Lehrer, R.I.; Lee, K.Y.C. Insertion selectivity of antimicrobial peptide protegrin-1 into lipid monolayers: effect of head group electrostatics and tail group packing. *Biochim. Biophys. Acta* **2006**, *1758*, 1450-1460.

29. Clifton, L.A.; Sanders, M.R.; Hughes, A.V.; Neylon, C.; Frazier, R.A.; Green, R.J. Lipid binding interactions of antimicrobial plant seed defense proteins: puroindoline-a and β-purothionin. *Phys. Chem. Chem. Phys.* **2011**, *13*, 17153-17162.

30. Sanders, M.R.; Clifton, L.A.; Neylon, C.; Frazier, R.A.; Green, R.J. Selected wheat seed defense proteins exhibit competitive binding to model microbial lipid interfaces. *J. Agric. Food Chem.* **2013**, *61*, 6890-6900.

31. Tran, D.; Tran, P.; Roberts, K.; Osapay, G.; Schaal, J.; Ouellette, A.; Selsted, M.E. (2008) *Microbicidal properties and cytocidal selectivity of Rhesus macaque theta defensins*. Antimicrob. Agents Chemother, *52*, 944-953.

32. Lipkin, R.B.; Lazaridis, T. (2015) *Implicit membrane investigation of the stability of antimicrobial peptide β-barrels and arcs.* J. Membrane Biol., *248***,** 469-486.

Figure Legends

Figure 1 Primary structures of the RTD-1 peptide (upper panel) showing the characteristic θ-defensin structural motif: a cyclic peptide backbone cross-linked by three (Cys-Cys) disulfide bonds, and the porcine protegrin-1, PG-1, (lower panel) which shows significant primary structural homology but has only two disulfides and no main chain cyclisation.

Figure 2 **(A)** Langmuir isotherms for 3:1 POPE:POPG monolayers spread at the air-water interface. The isotherm for the *d*-lipid system is shown in black, and that for the *h*-lipid system in red. (B) The change in surface pressure following addition of aRTD-1 to the *h*-lipid film (compressed to 25 mN/m and then held at constant area). The arrow indicates the time of peptide addition. (C) The corresponding plot showing the change in surface pressure following addition of PG-1 to the *h*-lipid film.

Figure 3 Neutron reflectivity data (shown as plots of $R(Q).Q^4$ *vs*. Q) and associated model fits for 3:1 POPE:POPG monolayers spread at the air-water interface, before (filled symbols) and after (open symbols) exposure to 0.48 μM aRTD-1. Data shown are for the three isotopic contrasts of *d*-POPE:POPG ± aRTD-1 on D_2O (A), *d*-POPE:POPG ± aRTD-1 on nrw (B), and *h*-POPE:POPG ± aRTD-1 on D_2O (C). The structural parameters used in providing the model fits shown are summarised in Tables 2 and 3.

Figure 4 Neutron reflectivity data (shown as plots of $R(Q).Q^4$ *vs*. Q) and associated model fits for 3:1 POPE:POPG monolayers spread at the air-water interface after exposure to 0.48 μM PG-1. Data shown are for *d*-POPE:POPG + PG-1 on D_2O (filled circles), *d*-POPE:POPG + PG-1 on nrw (open circles), and *h*-POPE:POPG + PG-1 on D_2O (open triangles). The structural parameters used in the model fits shown are summarised in Table 4.

Figure 5 (A) Scattering length density profiles for 3:1 d_{31}-POPE: d_{31}-POPG monolayers spread at the air-water interface and exposed to 0.48 μM PG-1 (dotted line) and aRTD-1 (solid line) (calculated on the basis of the neutron reflectivity model fits summarised in Tables 3 and 4). (B) Molecular model showing PG-1 inserted into a 3:1 POPE:POPG monolayer. The carbon atoms of the lipid acyl chains are shown in cyan, the peptide is

shown in white but with the arginine side chain guanidinium groups highlighted in violet, and the phospholipid N, O and P atoms shown in blue, red, and yellow, respectively. (C) Molecular model showing aRTD-1 inserted into a 3:1 POPE:POPG monolayer. The atom colours are as detailed for (B).

Table 1

Scattering lengths (Σ*b*), molecular volumes, and scattering length densities (ρ) of the molecular constituents of the various monolayers studied

Molecule/ fragment	Volume / Å^3	Scattering length density / 10^{-6} Å^{-2}
h-POPE:POPG acyl chains	909	-0.29
d-POPE:POPG acyl chains	909	3.26
POPE:POPG head groups	213	3.26
aRTD-1 in D_2O	2504	3.76
aRTD-1 in nrw	2587	1.99
PG-1 in D_2O	2504	3.91
PG-1 in nrw	2587	2.02

Table 2

Structural parameters obtained through simultaneous model fits to neutron reflectivity data obtained for 3:1 POPE:POPG monolayers at 25 mN.m^{-1} and 295 ± 2 K, before and after the injection of 0.48 μM aRTD-1 and PG-1 into the aqueous sub-phase.

		POPE:POPG	POPE:POPG + aRTD-1	POPE:POPG + PG-1
Layer 1	d† / Å	13		
	ρ / 10^{-6} Å^{-2}	3.26 (d_{31}-lipids) -0.29 (*h*-lipids)		
	% H_2O	0		
Layer 2	d† / Å	9	17.5	14
	ρ / 10^{-6} Å^{-2}	3.26	3.51 (D_2O) 2.63 (nrw)	3.68 (D_2O) 2.47 (nrw)
	% H_2O	33	50	39

† Layer thicknesses are given to the nearest 0.5 Å.

Table 3

Structural parameters obtained through simultaneous model fits to neutron reflectivity data obtained for 3:1 POPE:POPG monolayers at 25 mN.m^{-1} and 295 ± 2 K, after the injection of 0.48 μM aRTD-1 into the aqueous sub-phase.

3:1 POPE:POPG + aRTD-1				
		***d*$_{31}$-lipids / D$_2$O**	***d*$_{31}$-lipids / nrw**	***h*-lipids / D$_2$O**
Layer 1	d† / Å	16.5		
	ρ / 10^{-6} Å^{-2}	3.36	3.10	0.32
	% H$_2$O	0		
Layer 2	d† / Å	18		
	ρ / 10^{-6} Å^{-2}	3.45	2.78	3.45
	% H$_2$O	70		

† Layer thicknesses are given to the nearest 0.5 Å.

Table 4

Structural parameters obtained through simultaneous model fits to neutron reflectivity data obtained for 3:1 POPE:POPG monolayers at 25 mN.m^{-1} and 295 ± 2 K, after the injection of 0.48 μM PG-1 into the aqueous sub-phase.

3:1 POPE:POPG + PG-1				
		***d*$_{31}$-lipids / D$_2$O**	***d*$_{31}$-lipids / nrw**	***h*-lipids / D$_2$O**
Layer 1	d† / Å	16.5		
	ρ / 10^{-6} Å^{-2}	3.36	3.07	0.34
	% H$_2$O	0		
Layer 2	d† / Å	9		
	ρ / 10^{-6} Å^{-2}	3.46	2.89	3.46
	% H$_2$O	49		

† Layer thicknesses are given to the nearest 0.5 Å.

Table 5

Volume fractions of phospholipid, peptide and solvent in 3:1 POPE:POPG monolayers at 25 mN.m^{-1} and 295 ± 2 K, after the injection of 0.48 μM PG-1 and 0.48 μM aRTD-1 into the aqueous sub-phase.

	Volume fraction of layer after exposure to aRTD-1			Volume fraction of layer after exposure to PG-1		
	ϕ_P	ϕ_L	ϕ_S	ϕ_P	ϕ_L	ϕ_S
Layer 1	0.15	0.85	0	0.15	0.85	0
Layer 2	0.12	0.19	0.69	0.32	0.19	0.49

Figure 1


Gly.Phe.Cys.Arg.Cys.Leu.Cys.Arg.Arg
Arg.Thr.Cys.Ile.Cys.Arg.Cys.Val.Gly
Arg.Gly.Gly.Arg.Leu.Cys.Tyr.Cys.Arg.Arg
Arg.Gly.Val.Cys.Val.Cys.Phe.Arg

Figure 2A

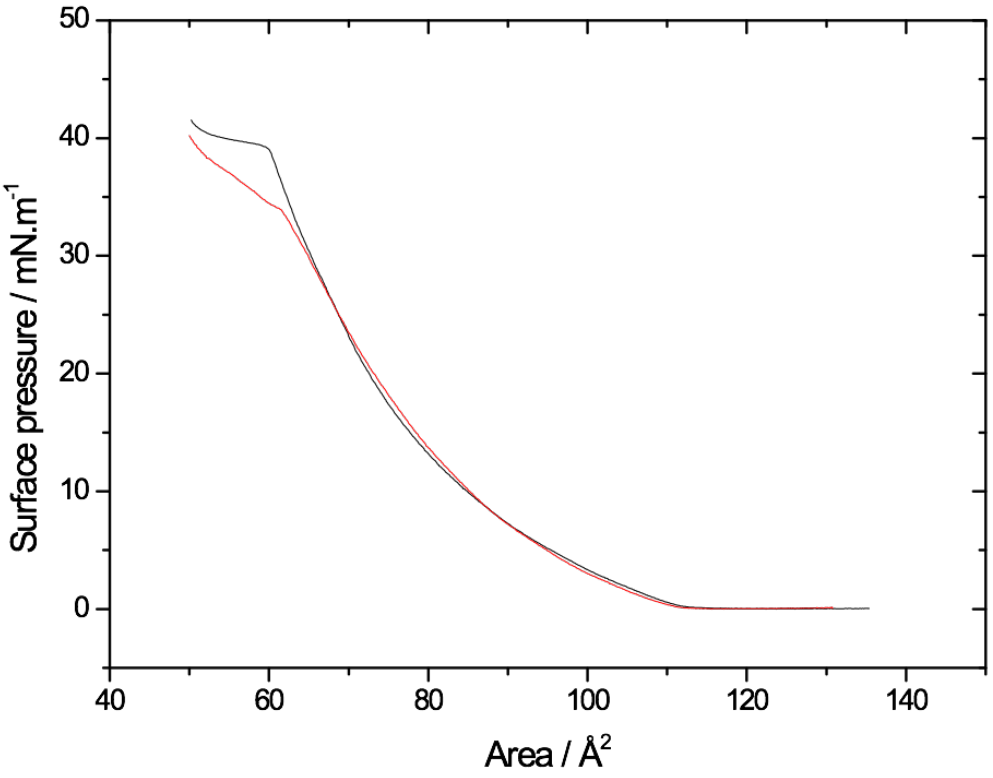
Surface pressure / mN.m-1
50
40
30
20
10
0
40
60
80
100
120
140
Area / Å2

Figure 2B

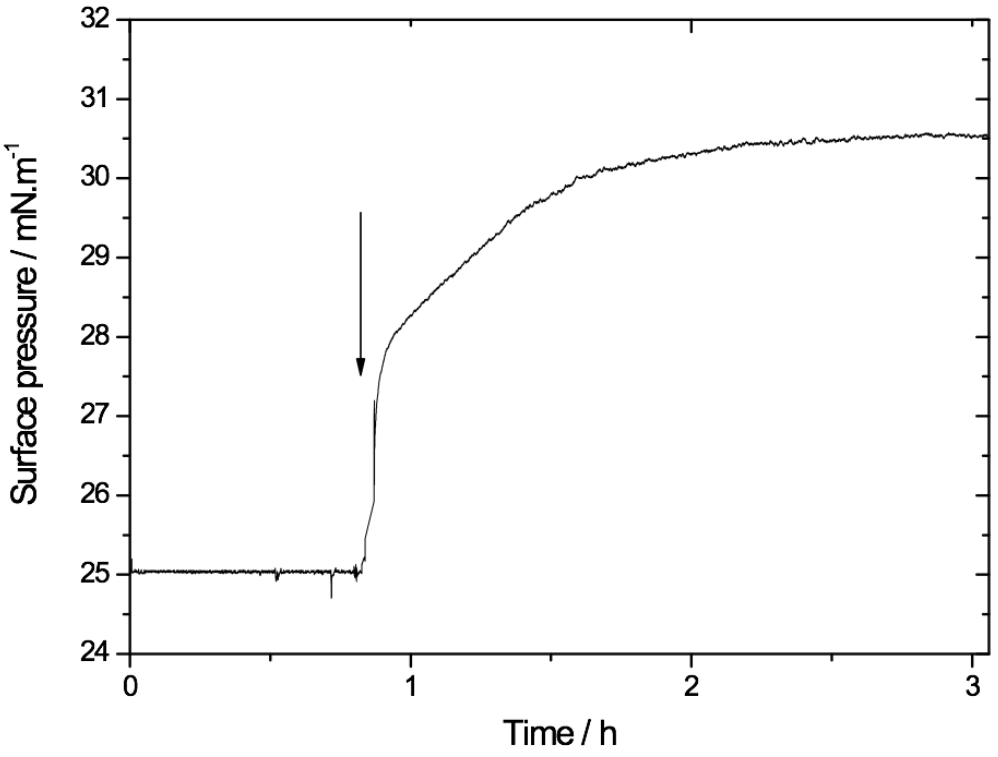

Figure 2C

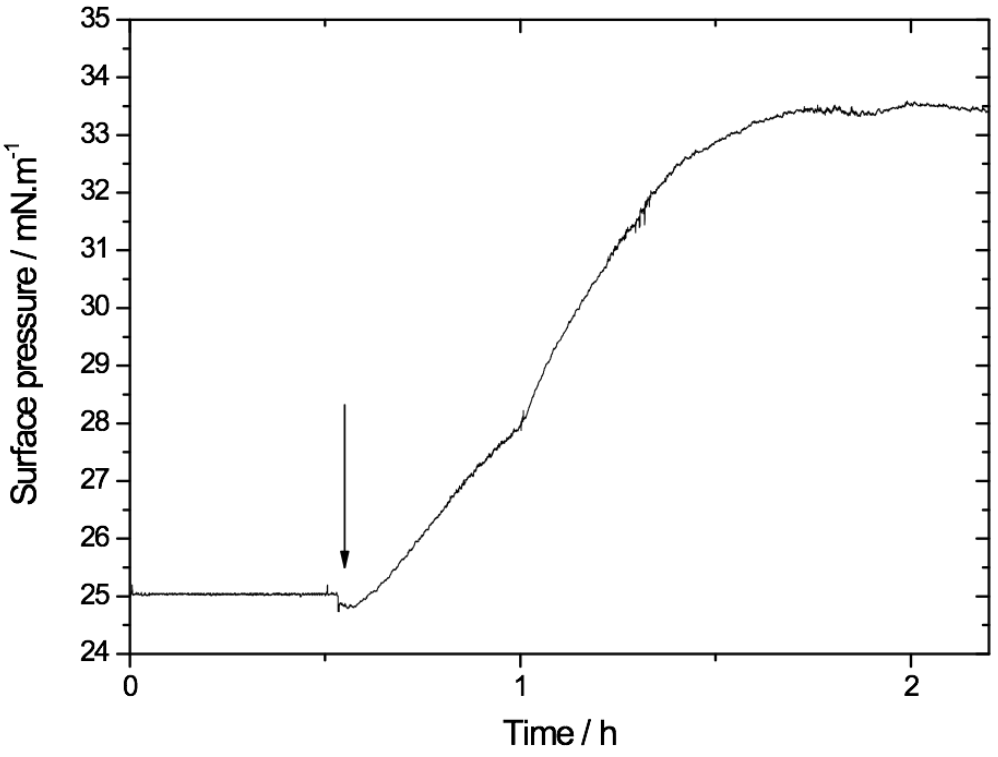
Surface pressure / mN.m-1
35
34
33
32
31
30
29
28
27
26
25
24
0
1
2
Time / h

Figure 3A

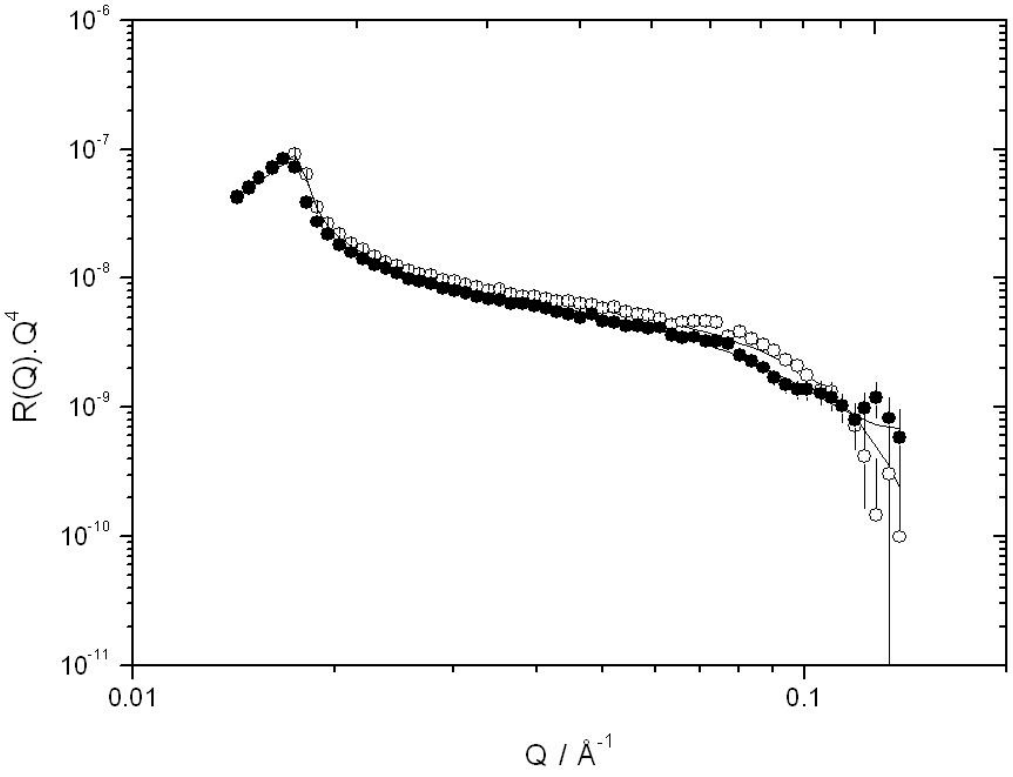

Figure 3B

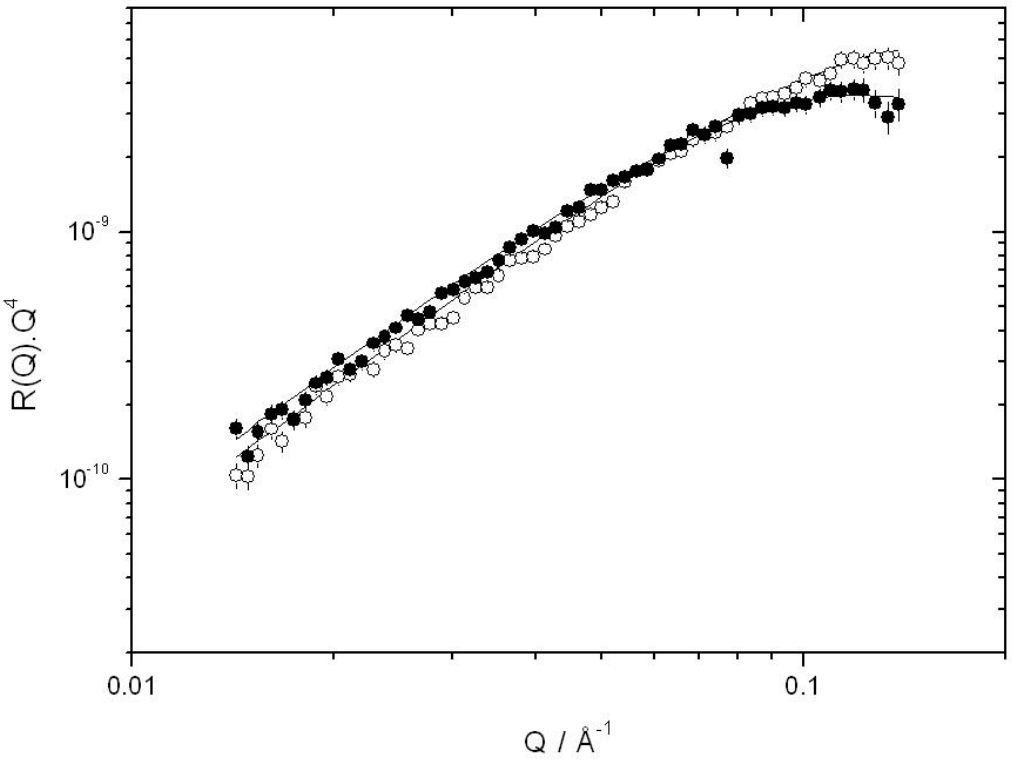

Figure 3C

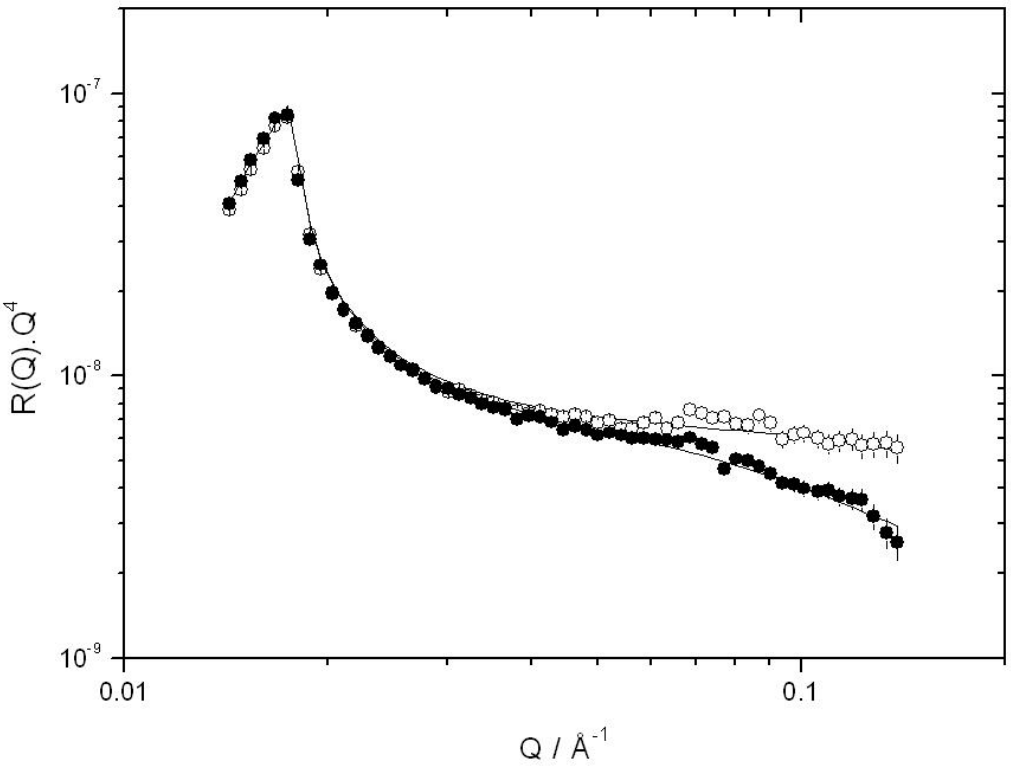

Figure 4

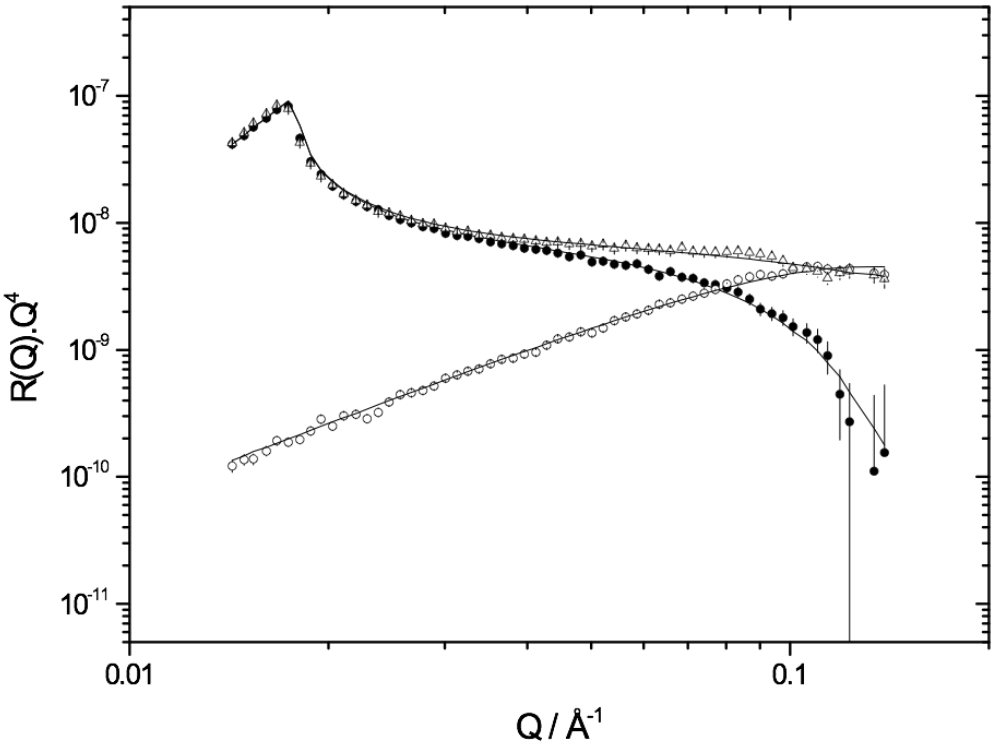

Figure 5A

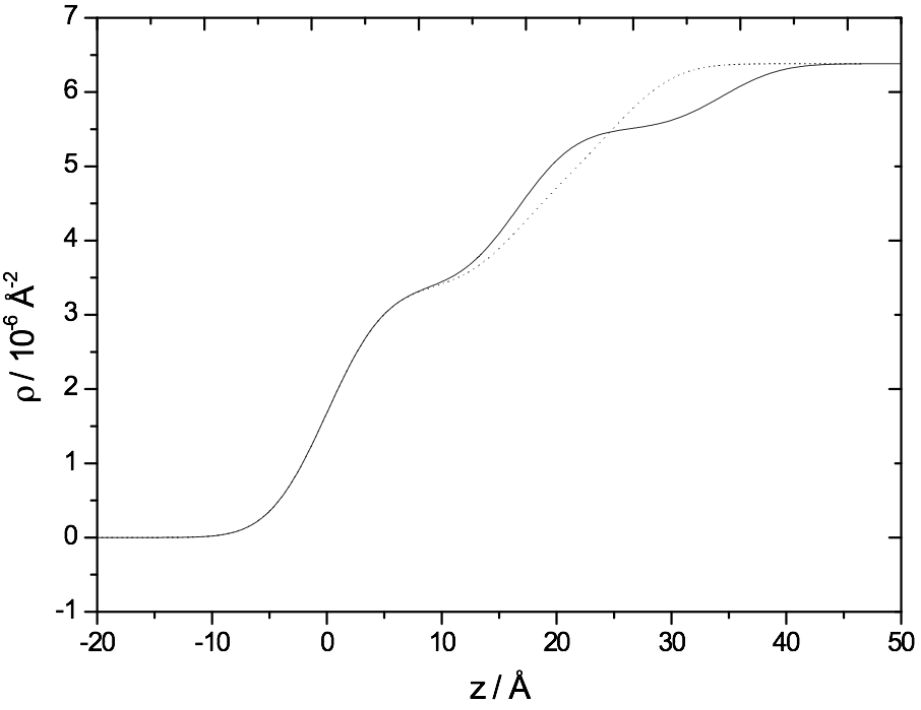

Figure 5B

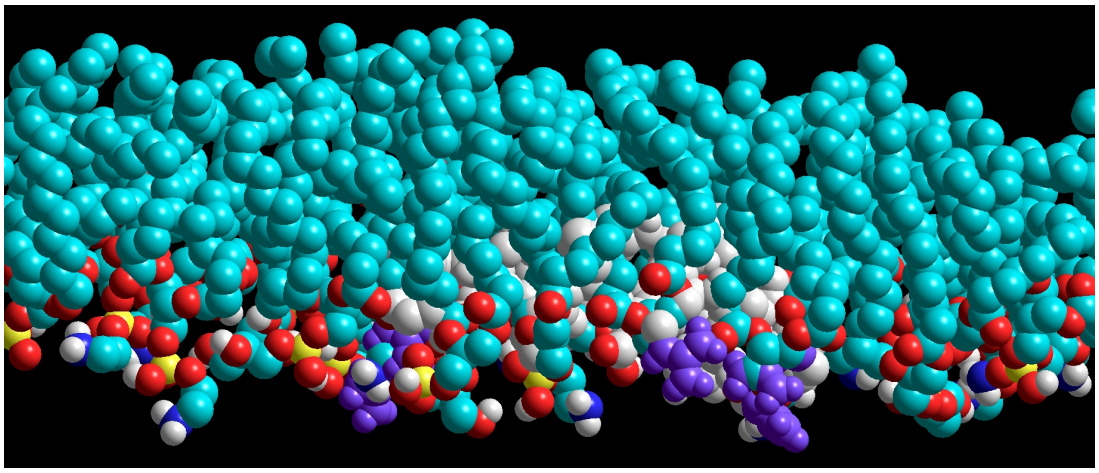

Figure 5C

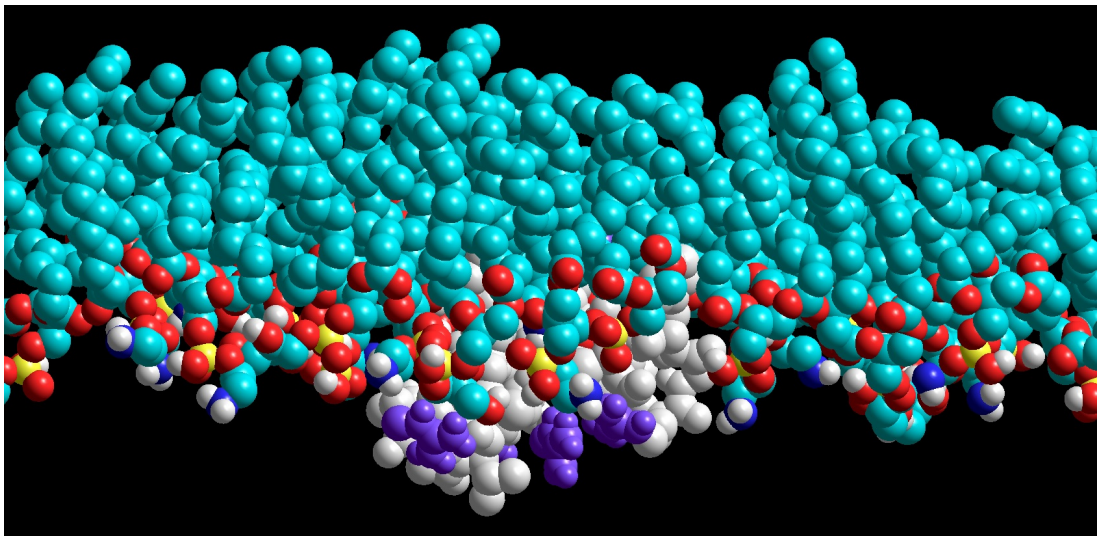

TABLE OF CONTENTS/ABSTRACT GRAPHIC